


CHARLES UNIVERSITY
Faculty of science

Behaviour of wet quartzite: deformation experiments revisited

Petar Pongrac[1], Petr Jeřábek[1], Holger Stünitz[2,3], Hugues Raimbourg[3], Lucille Nègre[3], Jacques Précigout[3]

[1]*IPSG, Faculty of Science, Charles University in Prague*

[2]*Department of Geosciences, University of Tromsø*

[3]*Institute of Earth Sciences, University of Orléans*

IPSG

UNIVERSITY OF TROMSØ

ISTO
Institut des Sciences de la Terre d'Orléans

Introduction

- After its discovery by *Griggs and Blacic* (1965), profound effect of water on mechanical strength of quartz at elevated temperatures and pressures has been well demonstrated in last century
- Implementation of H_2O fugacity term as the most recent improvement of the flow law (*Kohlstedt et.al.*, 1995)

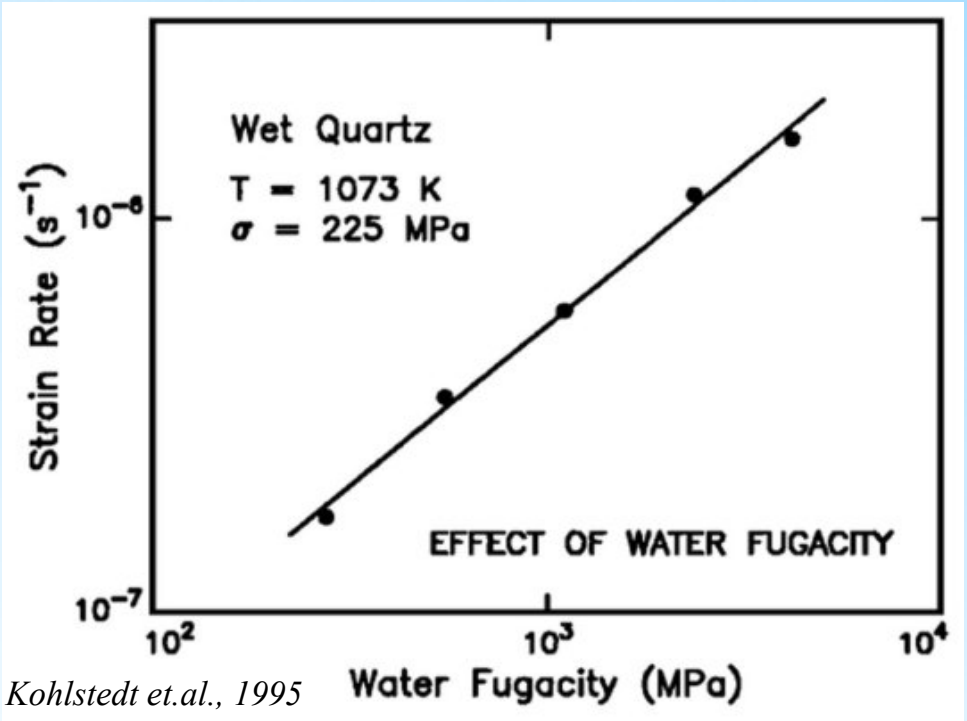

Kohlstedt et.al., 1995

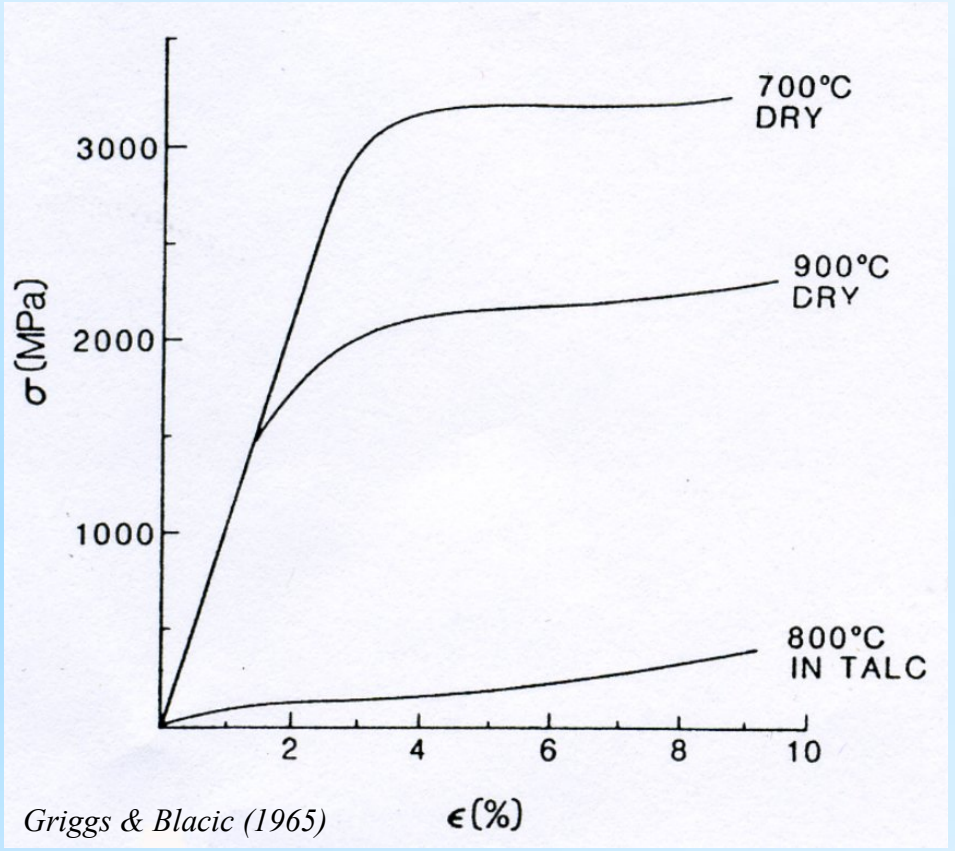

Griggs & Blacic (1965)

$$\dot{\varepsilon} = A\Delta\sigma^{n} f_{(H_2O)} e^{\frac{-Q}{RT}}$$

STRAIN RATE
STRESS EXPONENT
FUGACITY
ACTIVATION ENERGY
TEMPERATURE
GAS CONSTANT
DIFFERENTIAL STRESS
MATERIAL CONSTANT

Materials and Methods

Tana quartzite (northern Norway)

Samples: a) **as-is** – dried at 115 °C, no added H_2O

b) "**wet**" – dried at 115 °C, 0.1 wt% H_2O added

Deformation experiments: Griggs-type solid medium apparatus

EXPERIMENTAL SETTINGS:

	Axial shortening	**Strain rate stepping**	**Temperature stepping**
Number of experiments (as-is + wet)	4 + 4	3 + 3	1 + 1
Confining pressure	1 GPa	1 GPa	1 GPa
Temperature	900 °C	900 °C	750 850 °C 950
Strain rate	10^{-6} s^{-1}	10^{-5} 10^{-6} s^{-1} 10^{-7}	10^{-6} s^{-1}

Microstructure analysis:

a) optical microscopy b) CL imaging

c) EMPA elemental mapping d) EBSD analysis

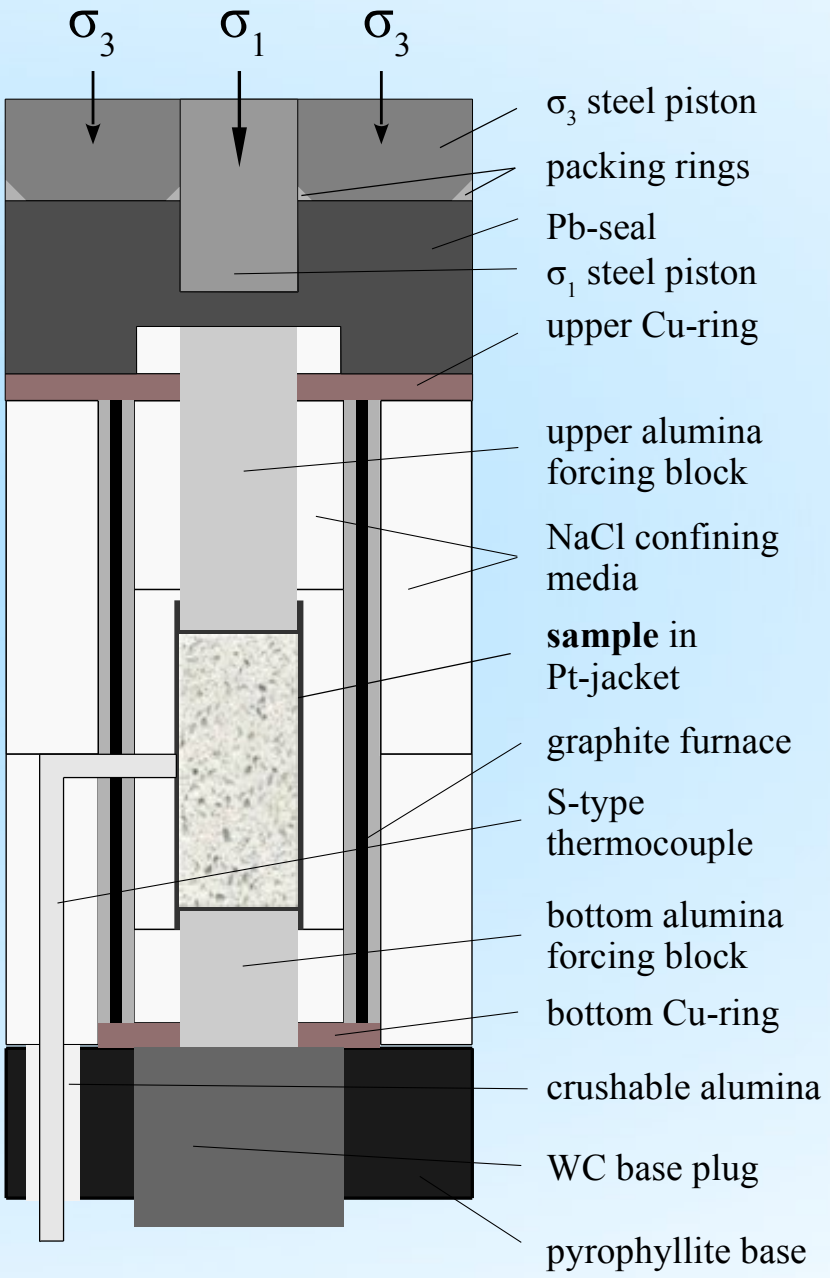

Results: **deformation**

Mechanical record of an entire axial shortening experiment:

a) pumping-up: progressive increase of pressure and temperature,

b) pre-deformation **pressurizing** (12 hours),

c) run-in: σ_1 piston displacement starts; loading and penetration through Pb-seal,

d) σ_1 piston is getting in touch with forcing block in assembly; **hit point** evaluation and start of deformation,

e) constant **deformation**,

f) quenching and depressurizing.

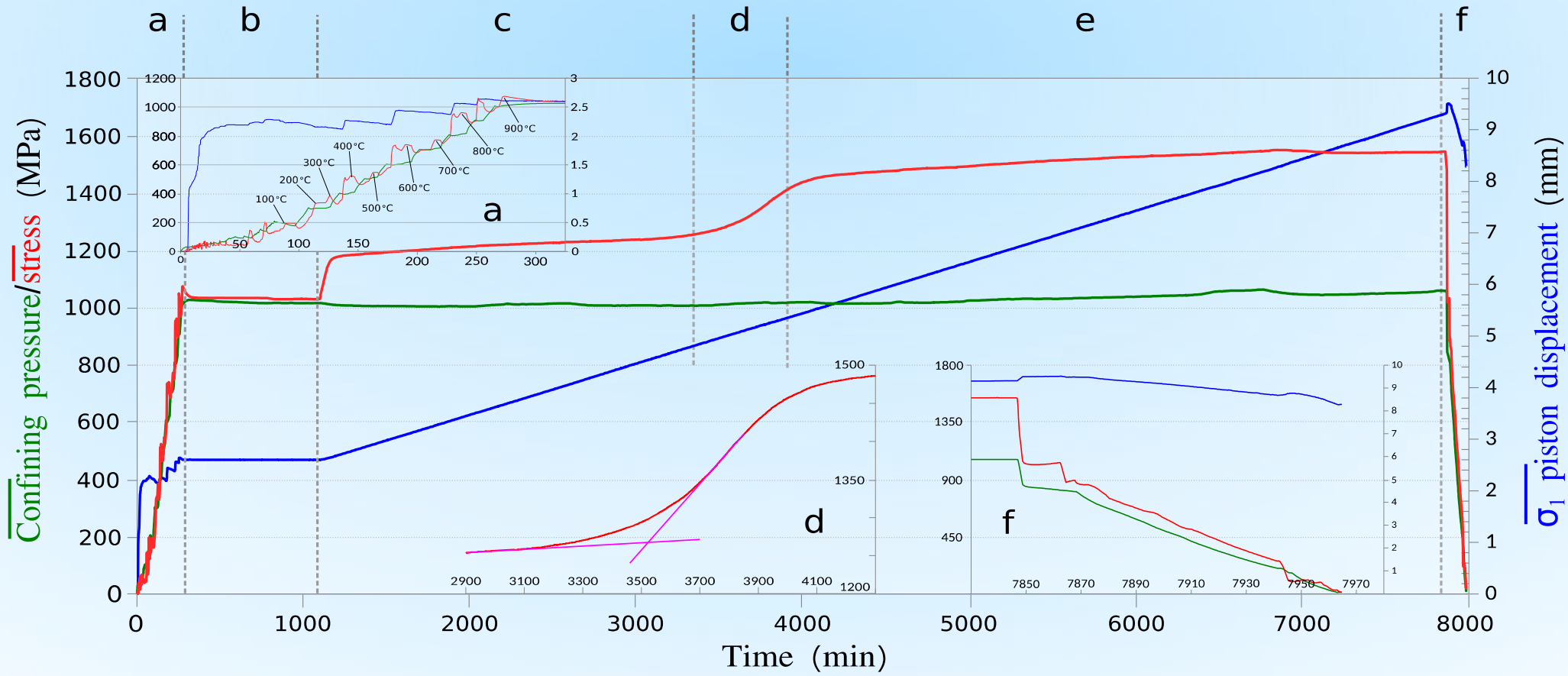

Results: **mechanical properties**

- Strain-stress curves for all axial shortening experiments
- Stress values evaluated using corrections of *Holyoke & Kronenberg* (2010)
- Average differential stress values are presented with blue (as-is) and red (wet) lines

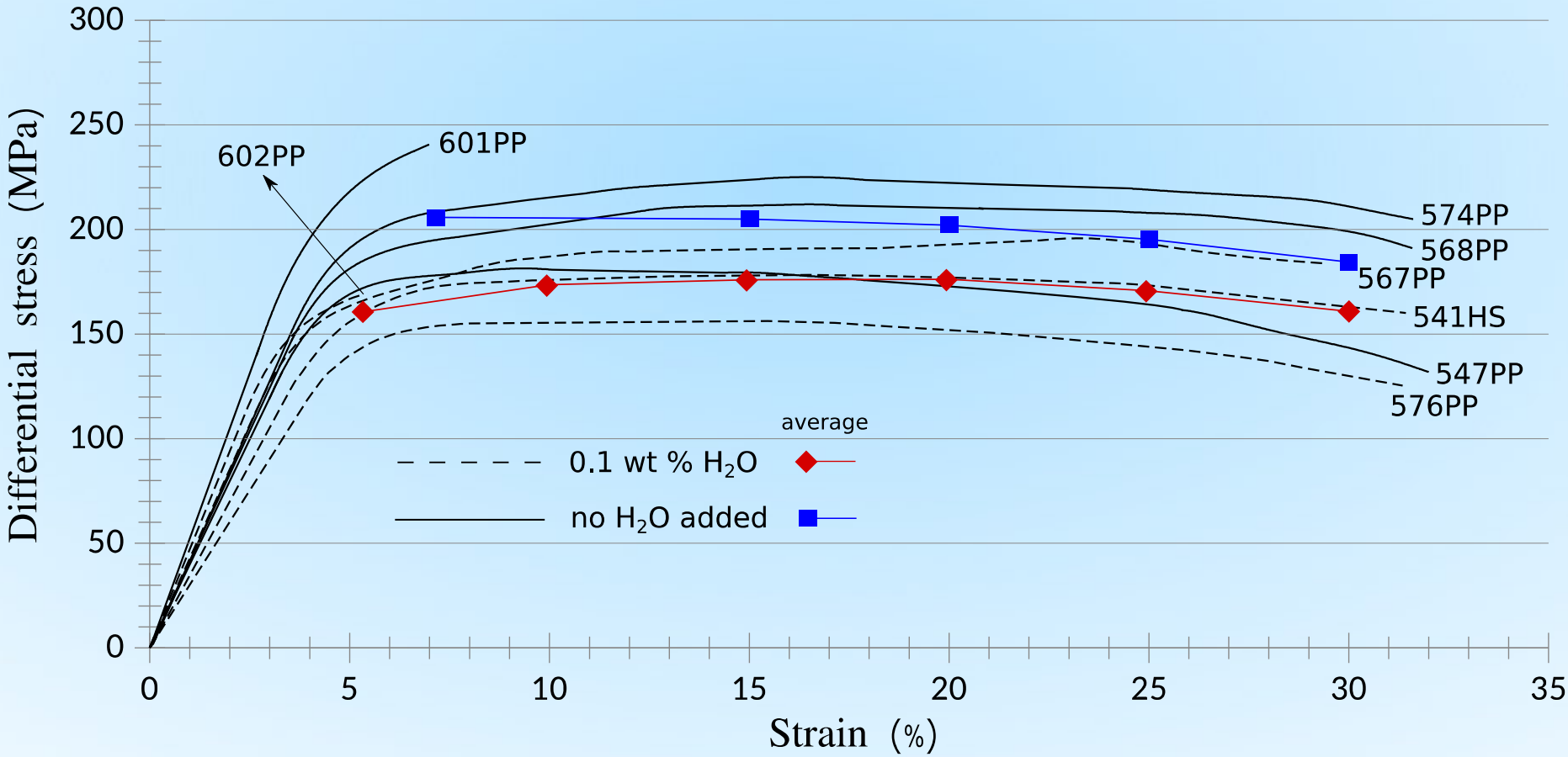

Results: **strain rate stepping**

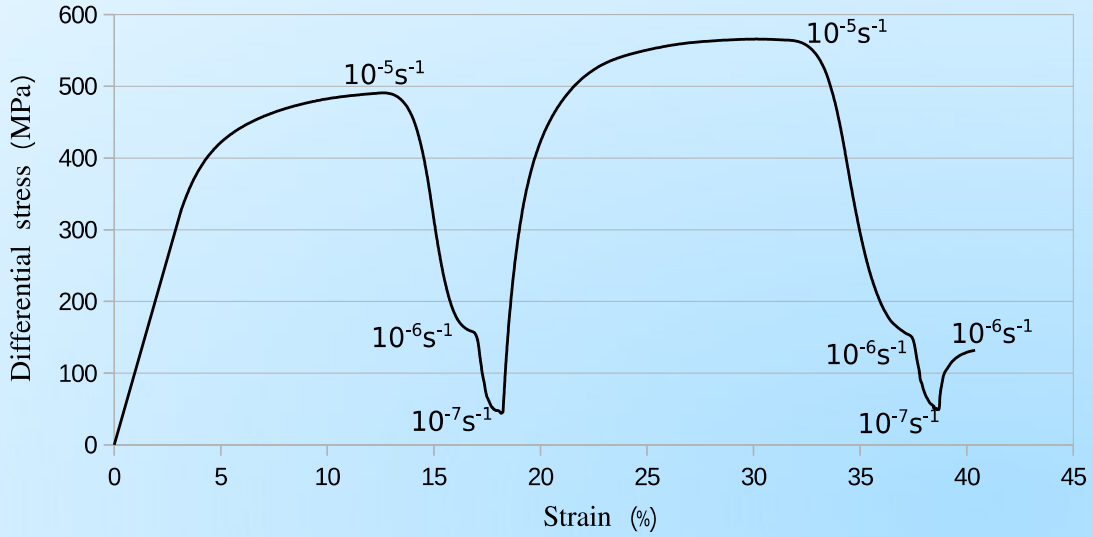

- Representative stress-strain curve for a strain rate stepping experiment
- Strain rate was changing as shown, but not necessarily in the same order for all experiments

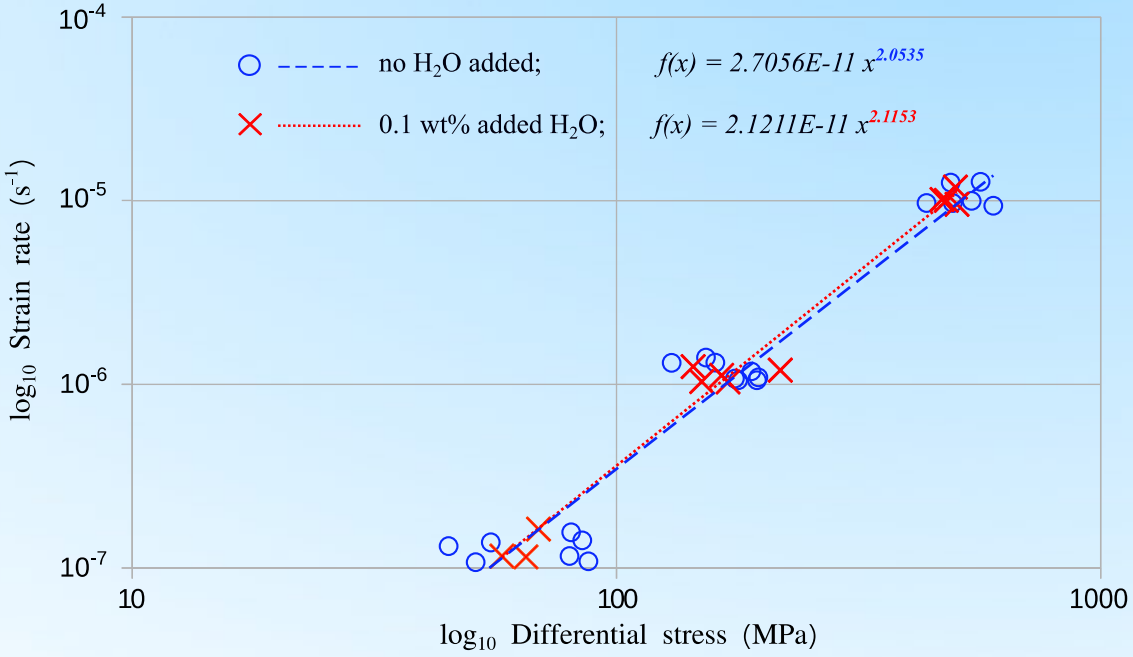

- Strain rate stepping results in summary, including data from all SRS experiments
- Values of stress exponents:
  - $n_{as\text{-}is} = 2.0535$
  - $n_{wet} = 2.1153$

Results: **temperature stepping**

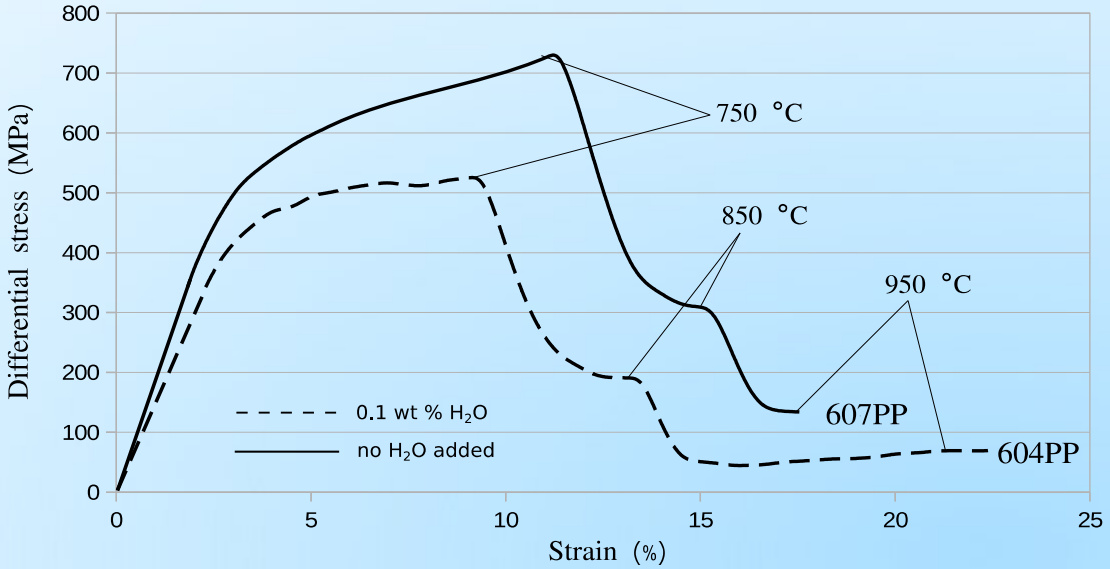

- Stress-strain curves for as-is and wet temperature stepping experiment
- Stress values for activation energy calculation at each step were taken from marked spots of the curves

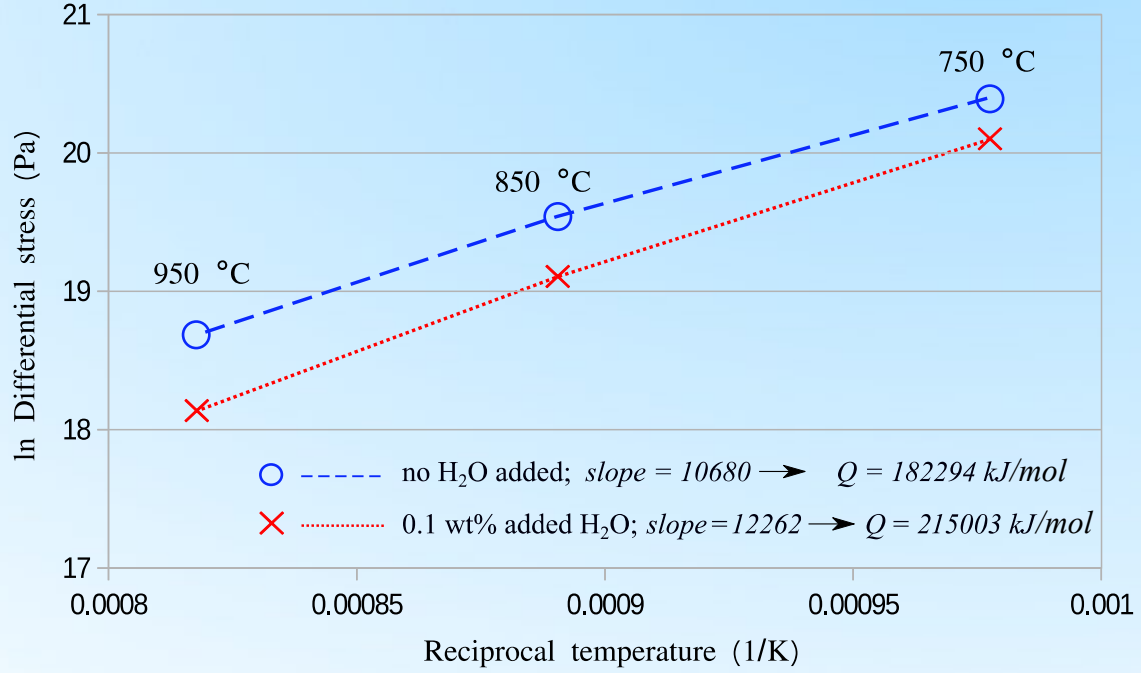

- Temperature stepping results plotted as inverse temperature versus *ln*-differential stress as well as calculated activation energy *Q*
- Activation energy *Q* (shown at the bottom) values were obtained by multiplying slope values with gas constant *R* and previously evaluated stress exponents *n*

Results: microstructure – **starting material**

- **Representative microstructure of the starting material:**

A) optical image in **cross-polarized light**, showing mosaic-like microstructure (red square marks the area shown on images E and F),

B) **thermionic CL** image (RGB), distinguishing initial sand grains (yellow-light brown) and cement between them (dark brown-black),

C) and D) **microprobe Al and K maps**, showing relative differences in Al and K content (remark: due to measuring resolution, the width of concentration maxima is exaggerated),

E) magnified area (red square on image A) showing typical mica distribution along the grain boundaries and junctions,

F) **back-scattered electrons** image of the image E area, showing grain boundary contamination with accessory mica phases, corresponding to Al and K maxima.

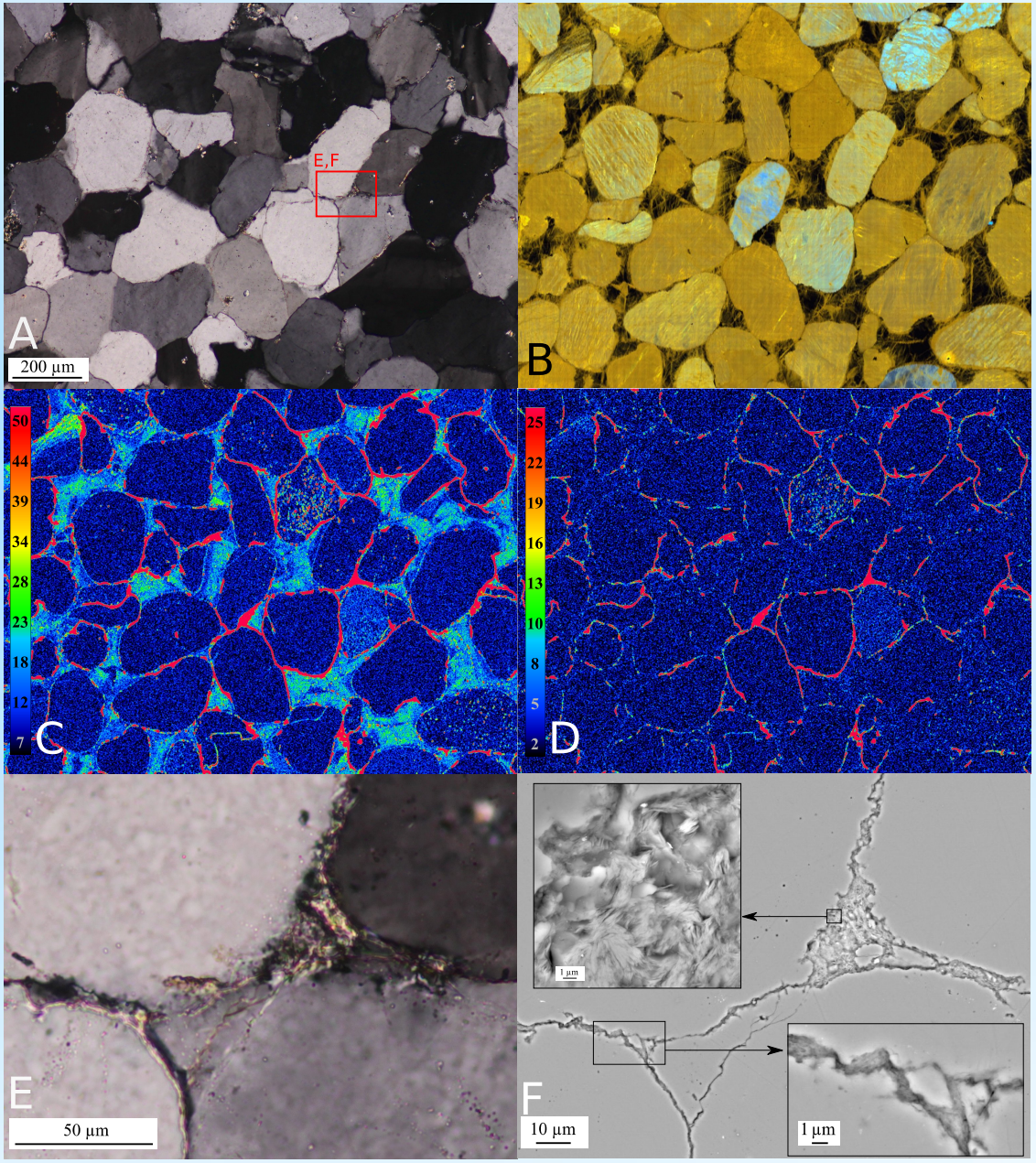

Results: microstructure – **after the experiment**

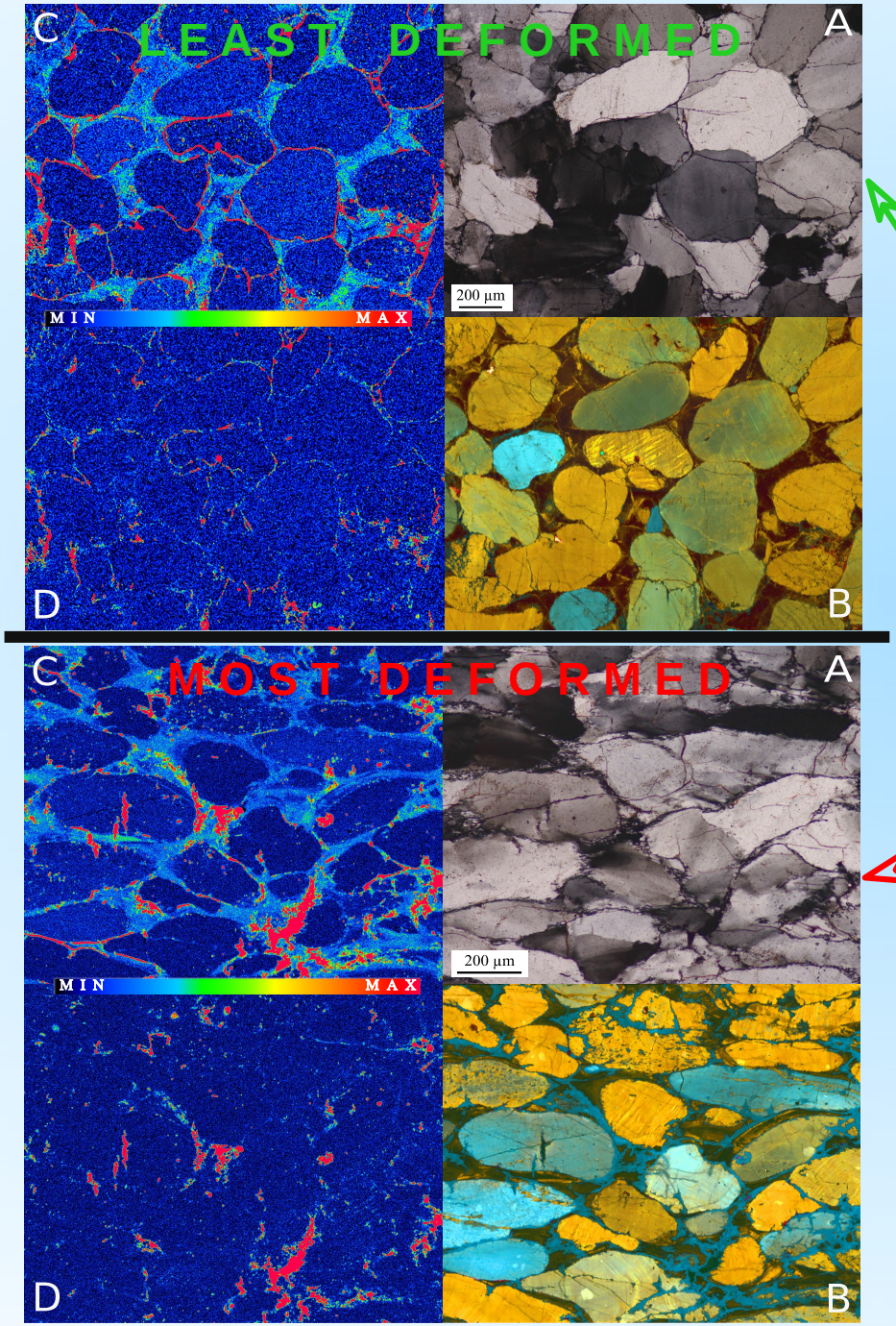

Differences in microstructure of the least and most deformed parts of a sample after the experiment:

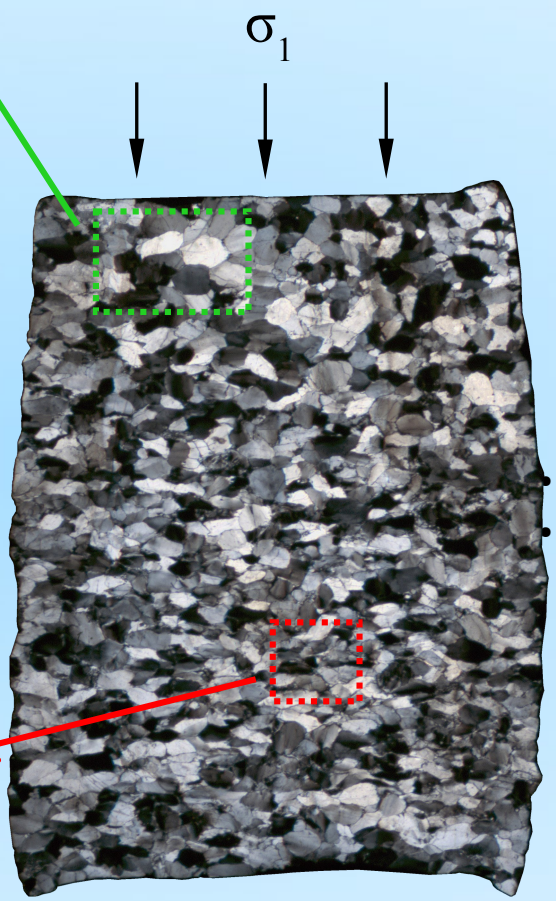

A) microstructural differences determined in **cross-polarized light:** different level of deformation visible in least and most deformed part according to 1) occurrence of newly formed (small) grains, 2) undulatory extinction and 3) grains flattening and shape preferred orientation perpendicular to σ_1 direction,

B) microstructural differences visible in **thermionic CL:** light blue luminescence in cement zone appeared in the most deformed part image as a result of recrystallization (either in cracks or cement zone); small dark-brown grains are relicts of cement fragments,

C) and D) **EMP Al and K maps**, showing redistribution of Al- and K-bearing phase from the form of rims around original sand grains (still preserved in least deformed part) to the clusters appearing mostly in recrystallization domains in most deformed part.

Results: microstructure – **most deformed part**

Common microstructure features in the most deformed part (red squares mark EBSD analyzed area): A) newly formed small grains visible in cross-polarized light, B) thermionic CL image distinguishes recrystallized grains and/or subgrains (blue luminescence) from relicts of cement (dark brown), and detects fluid pockets and cracks propagation, C) EMPA-Al map, showing Al concentration maxima in correspondence with visible fluid pockets, D) BSE image; blue circle points out the former fluid phase, E) raw EBSD map shows recrystallization regions and orientation relation and F) internal misorientation map with inner (yellow; boundaries of internal misorientation reflecting lattice distortion) and subgrain (red; misorientation angle between 2° and 10°) boundaries.

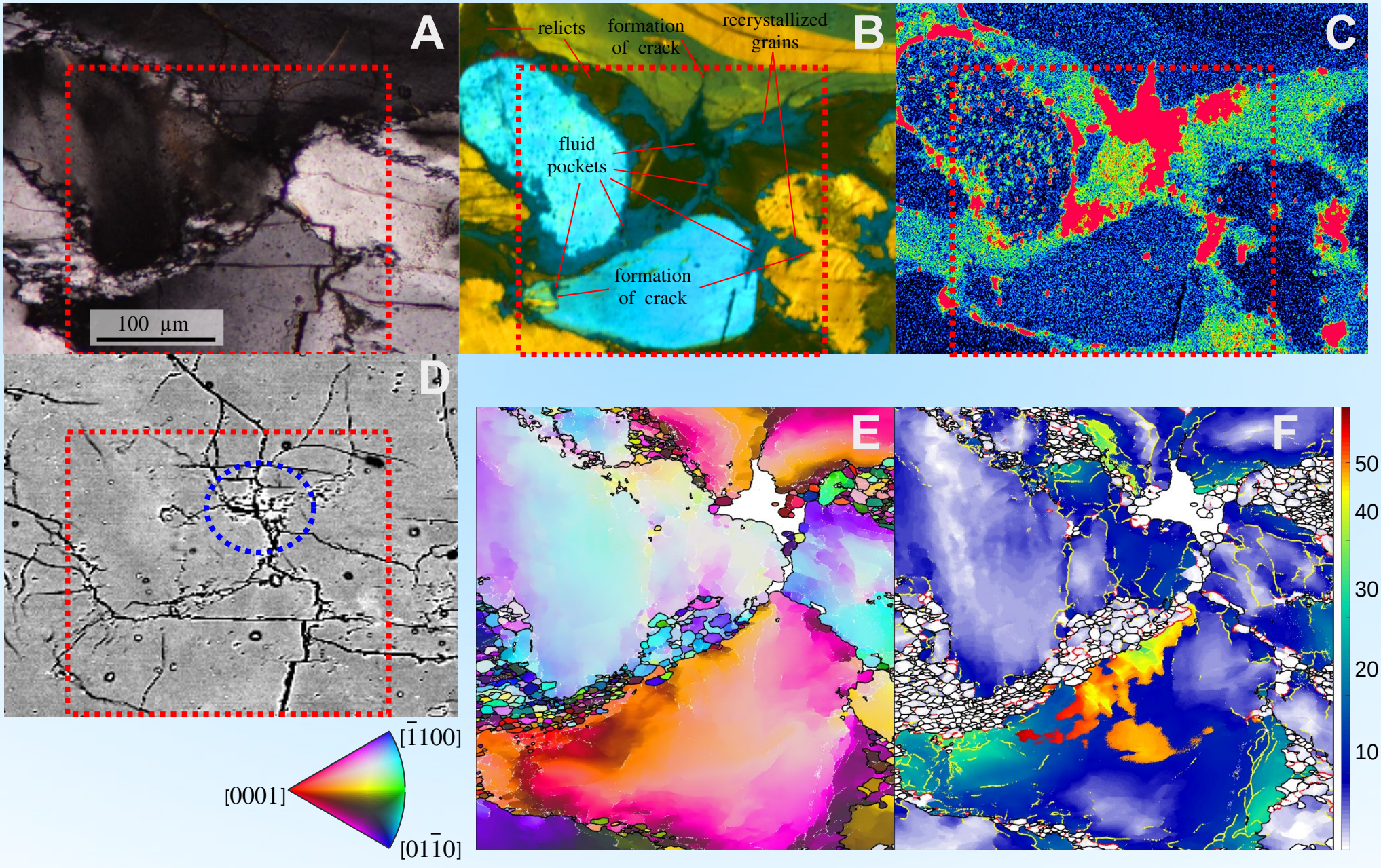

Results: microstructure – **domains of newly formed grains**

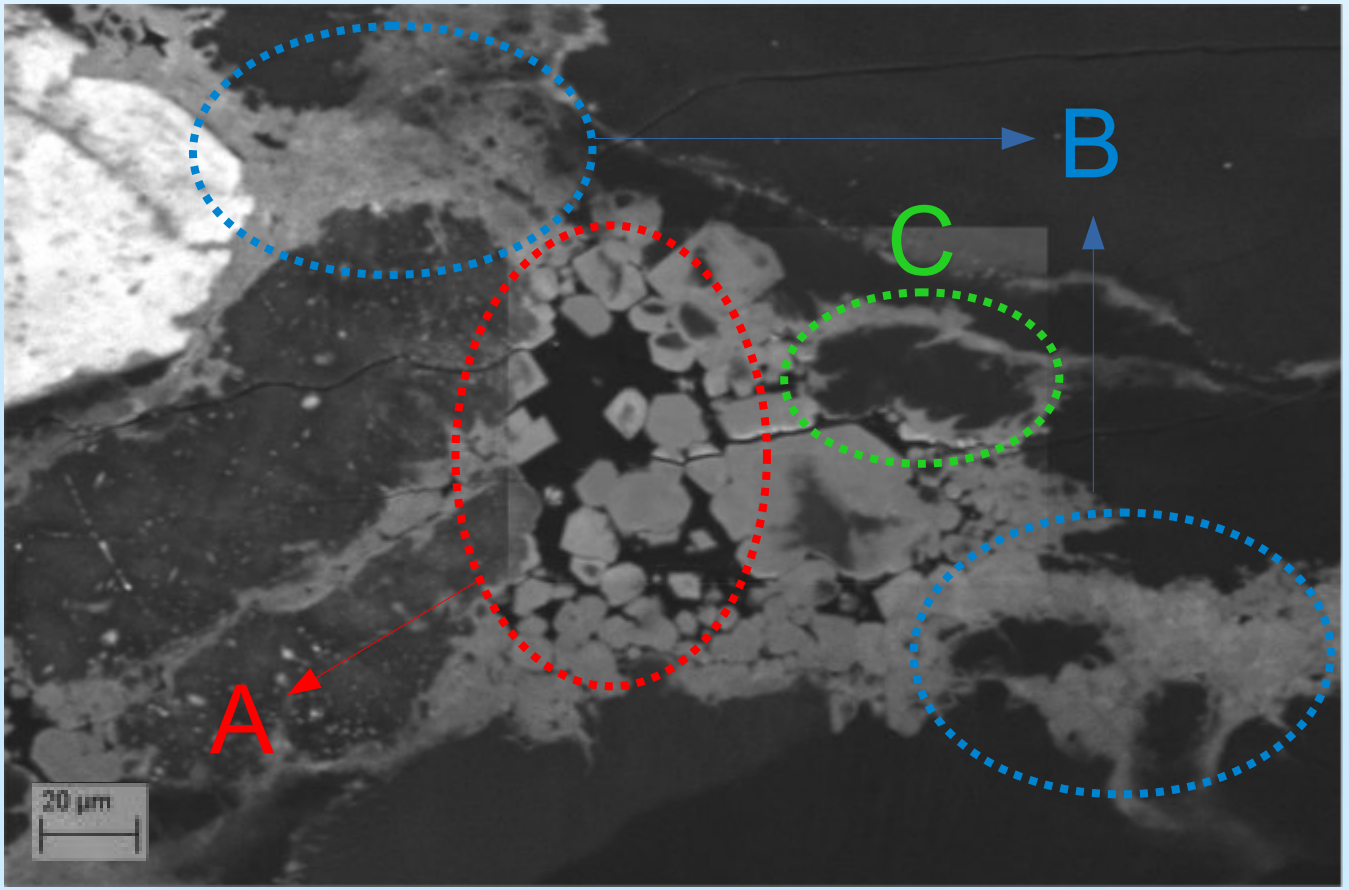

- **Three main features of newly formed grains domains demonstrated on monochromatic CL image:**

  A) fluid pocket with cracked grain fragments, often showing subhedral to euhedral outline of the overgrowth edges

  B) new grains formed by recrystallization (2 – 5 µm in size)

  C) a relict of cement fragment of the parent grain

Results: EBSD – **subgrain rotation recrystallization**

Orientation profiles show gradual and systematic change of recrystallized grains orientation between two parent grains. Misorientation angle is with respect to starting point (0 μm).

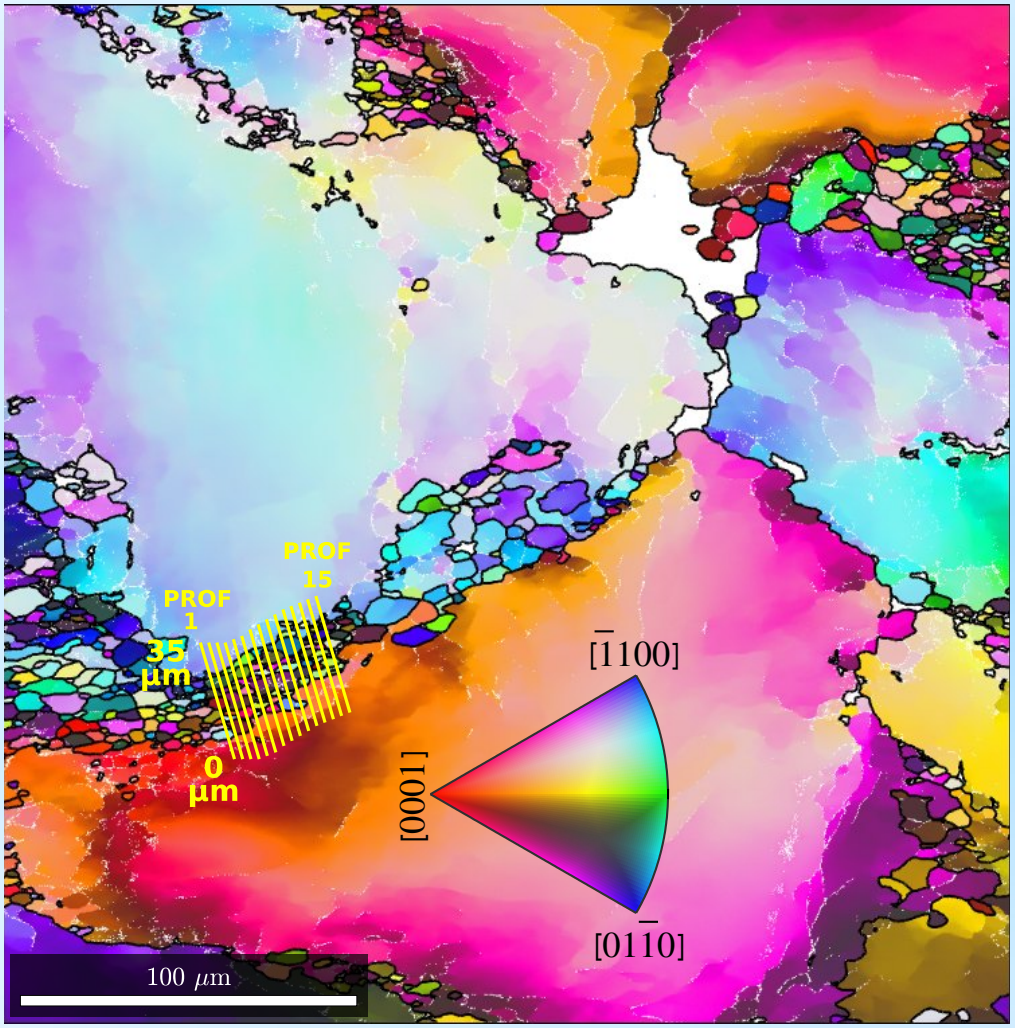

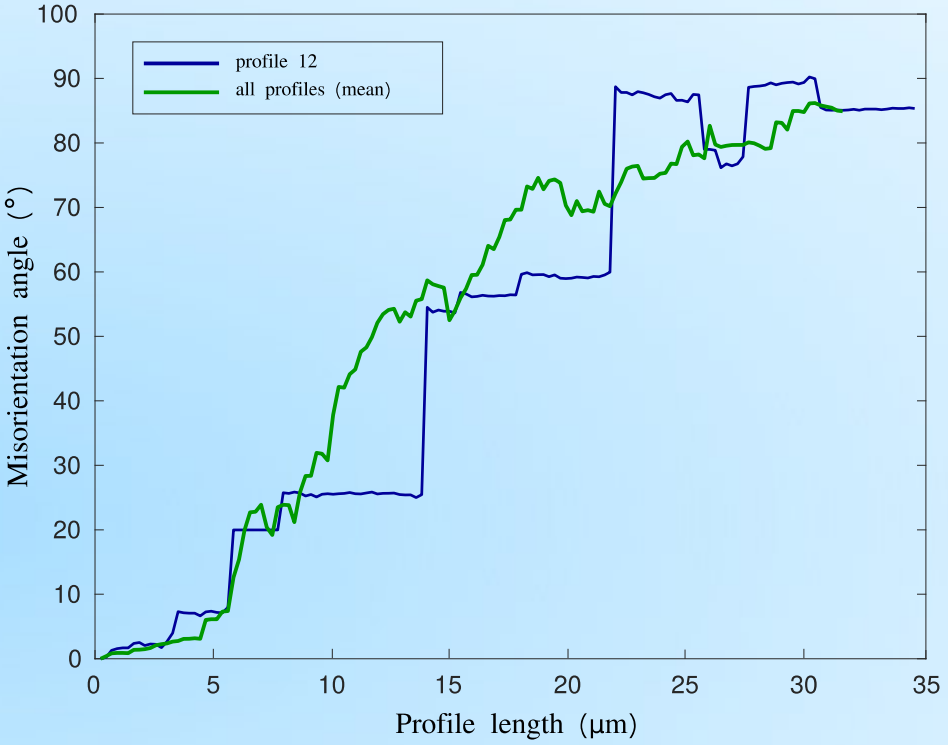

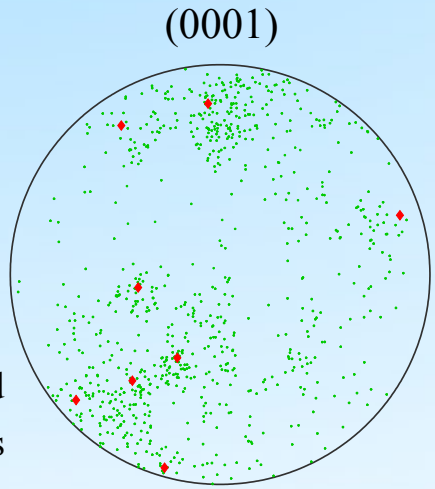

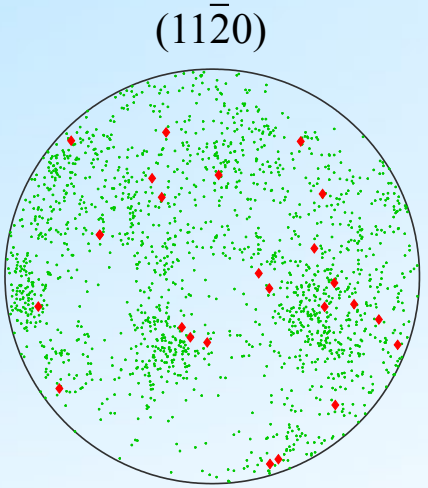

Pole figures present similar orientation of newly recrystallized (green dots) and parent (red diamonds) grains

Results: EBSD - **analysis of tilt boundary rotation axes**

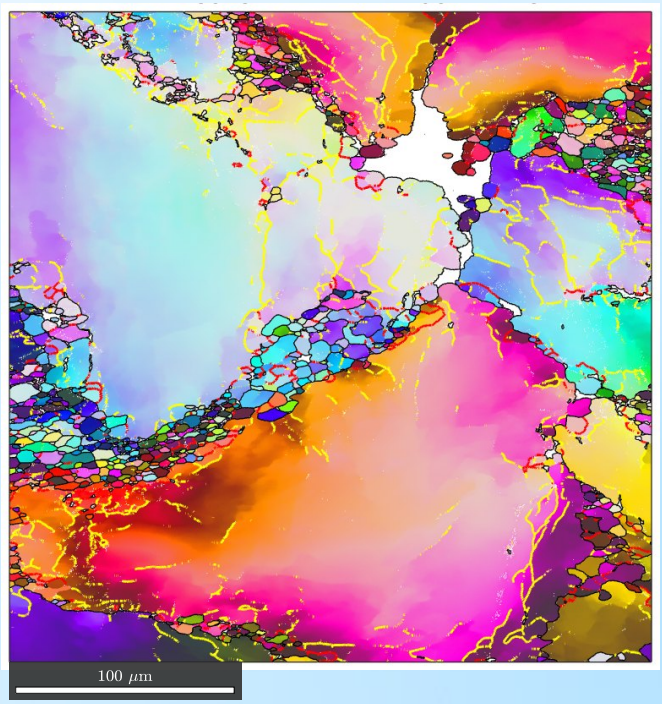

Yellow – inner boundaries
Red – subgrain boundaries

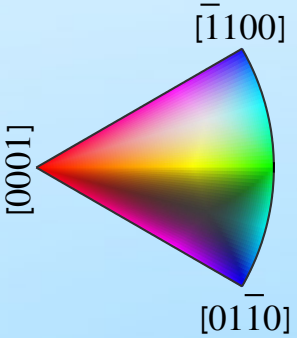

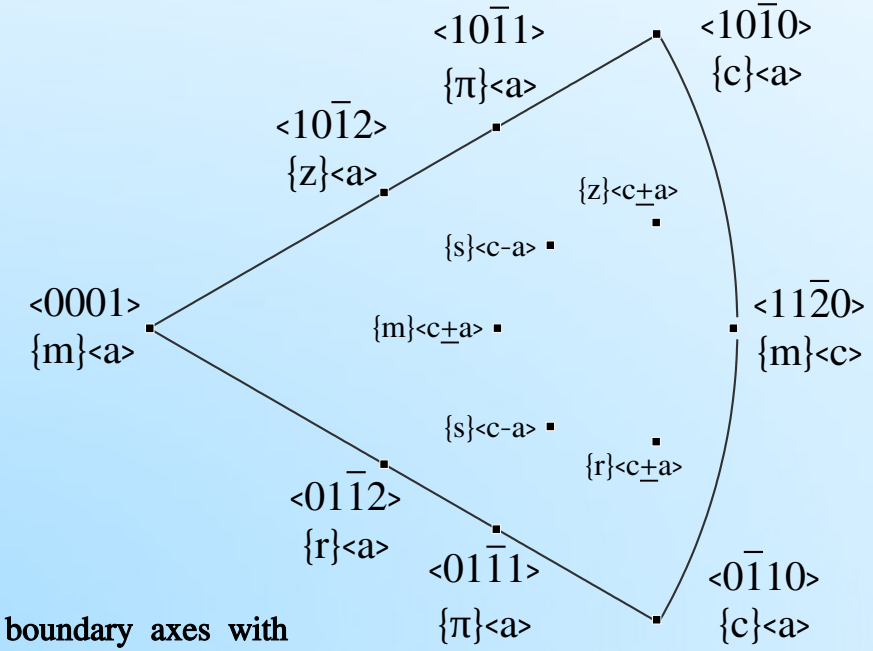

Orientation of tilt boundary axes with correspondent slip system and direction

from: Kilian & Heilbronner (2017)

Inner boundaries

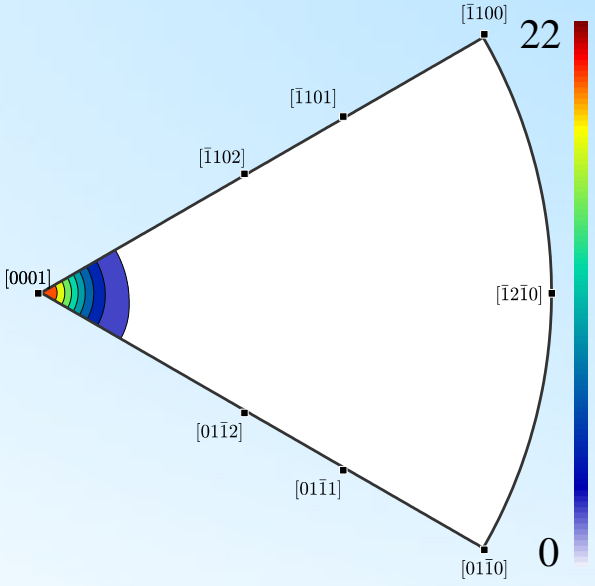

Subgrain boundaries

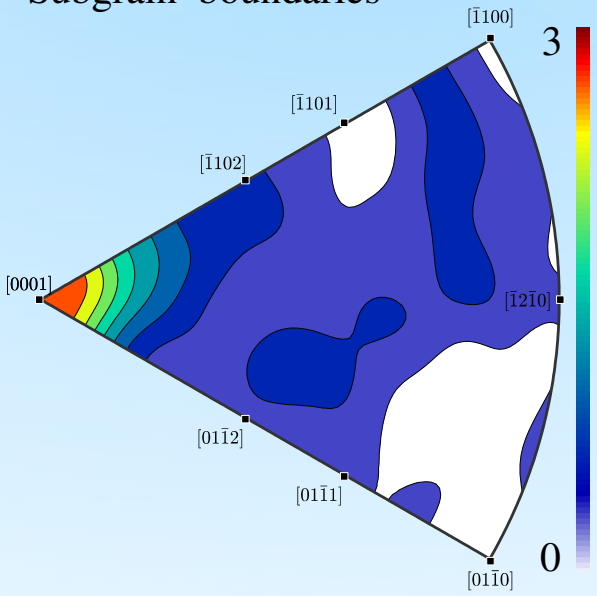

Inner + subgrain boundaries

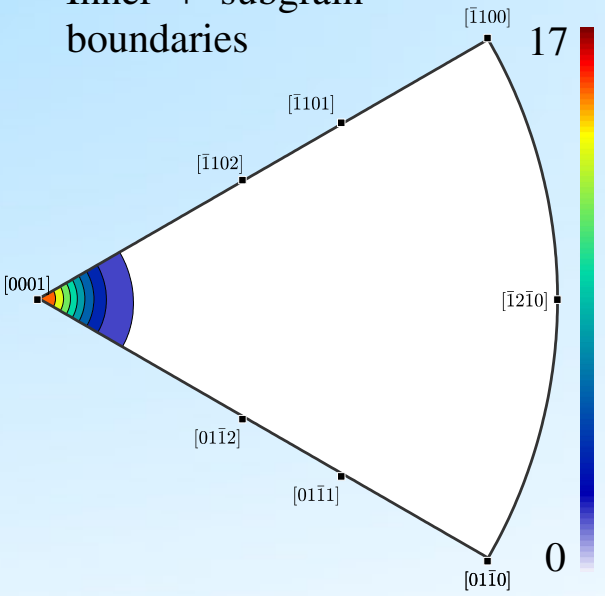

Results: EBSD – **slip system activation and Schmid factor dependence**

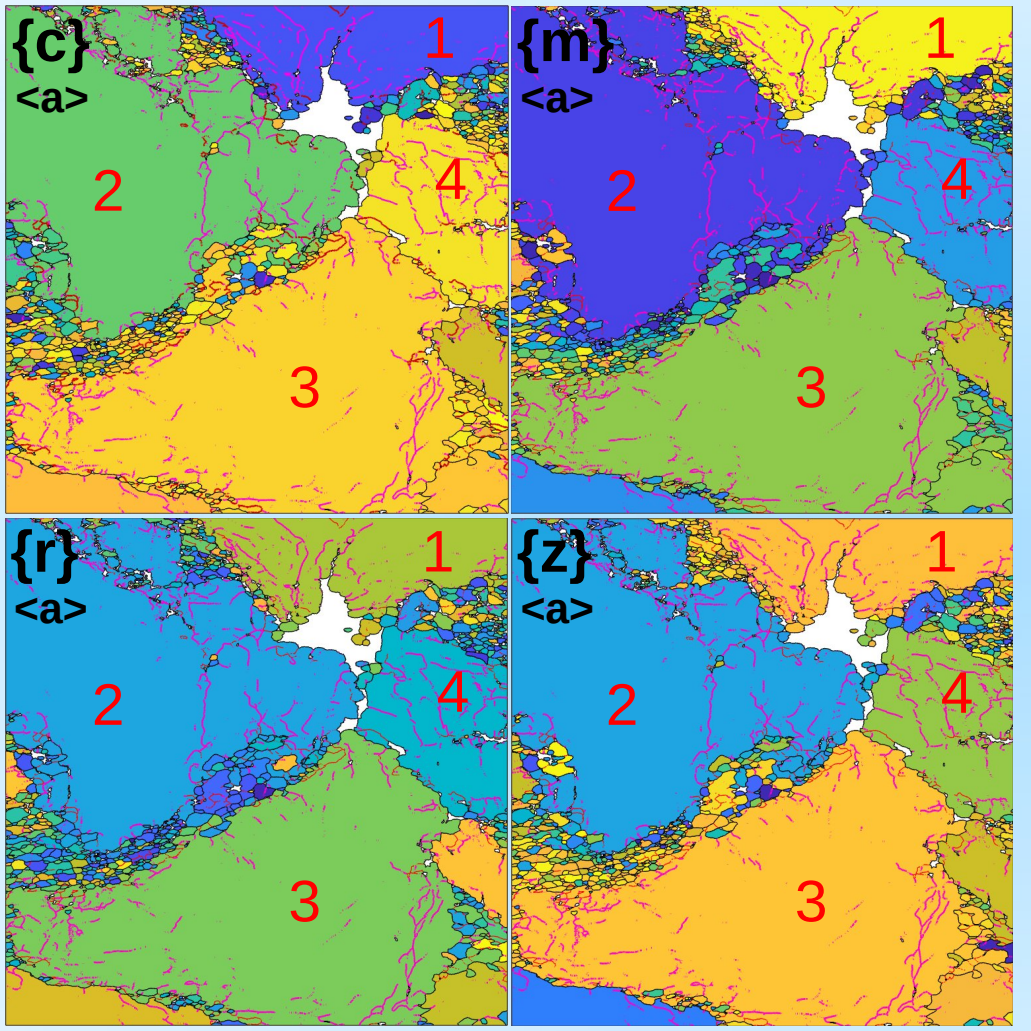

Slip systems: **{c}** – basal; **{m}** – prism; **{r}** – positive rhomb; **{z}** – negative rhomb; with glide direction **<a>**.

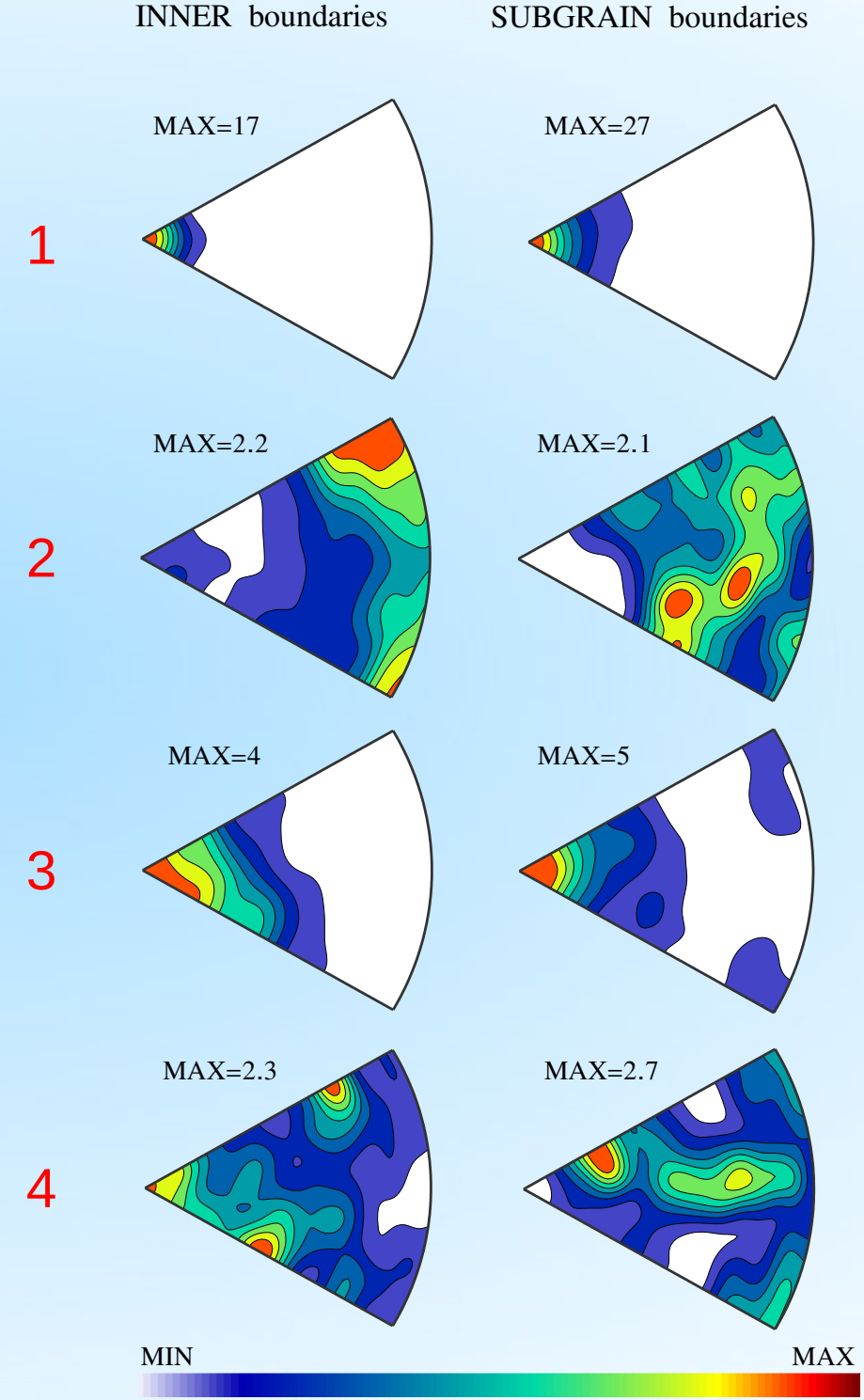

Conclusions (1)

- Although wet samples have systematically shown slightly lower average strength, amount of 0.1 wt% added H_2O had no distinct effect on mechanical stability.

- Strain rate stepping experiments gave surprisingly low stress exponent values of 2.05 (as-is) and 2.14 (wet)

- Temperature stepping gave activation energy of 182294 kJ/mol (as-is) and 215003 kJ/mol (wet)

- Even though starting material is considered extremely clean and bulk content of mica appears to be very low, the important fact is that mica minerals are distributed mostly along the boundaries between original sand grains and cement. After their disintegration under the experimental conditions, generated melt is with addition of H_2O forming a fluid phase that is being redistributed and found in clusters in the most deformed part of samples. Accordingly, the question appears, at which extent the fluid phase can affect bulk mechanical behavior while migrating through sample (as traced by Al and K concentration peaks) and promoting fragmentation. However, the fluid phase is eventually collected and quenched in the stress relaxed zones such as crack openings and recrystallized regions at triple points.

- Microstructure of the most deformed region of sample after experiment is characterized by 1) flattened and sometimes cracked parent grains with distorted undulatory extinction and shape preferred orientation perpendicular to the principal stress and 2) domains of newly formed grains. Domains of newly formed grains consist of 1) recrystallized grains 2 – 5 μm in size, 2) relicts of parent grains in form of cracked fragments of cement, some of which are overgrown by crystallization rim and 3) clusters of quenched melt/fluid.

Conclusions (2)

- Orientation profiles and pole figures have demonstrated similar orientation of parent grains and newly formed recrystallized grains, pointing to subgrain rotation as the main recrystallization mechanism.

- EBSD data revealed priorities between slip system, in order: {m}<a> > {r}<a>, {z}<a> > {c}<a>.

  Grain 1 confirms that highest Schmid factor for prism slip system usually excludes other systems to activate, and tilting axes of the most boundaries correspond to prism <a> slip.

  Grain 2 shows basal system activation when Schmid factor for all other systems is fairly low.

  In grain 3, even though Schmid factor for basal <a> and negative rhomb <a> slip is at around 0.45 and for prism <a> only 0.3, most boundaries are tilting in prism slip system, with exception of several subgrain boundaries related to the basal slip.

  Grain 4 shows priority of both positive and negative rhomb <a> over basal <a> slip, even Schmid factor is considerably higher for the basal. Priority between two rhombs is not clear.

REFERENCES

- Griggs, D.T., Blacic, J.D. (1965): Quartz: anomalous weakness of synthetic crystals. Science 147, 292–295.
- Holyoke, C. W. and A. K. Kronenberg (2010): Accurate differential stress measurement using the molten salt cell and solid salt assemblies in the Griggs-apparatus with applications to strength, piezometers and rheology, Tectonophysics, 494(1), 17–31.
- Kohlstedt, D.L., Evans, B., Mackwell, S.J. (1995): Strength of the lithosphere: constraints imposed by laboratory experiments. J. Geophys. Res. 100, 17587–17602.
- Kilian, R., Heilbronner, R. (2017) : Analysis of crystallographic preferred orientations of experimentally deformed Black Hills Quartzite. Solid Earth, 8, 1095–1117.

ACKNOWLEDGEMENTS

- Research project is financially supported by *Charles University Grant Agency* (GAUK) and *University Centre of Excellence* (UNCE)